Deep Learning for Interictal Epileptiform Discharge Detection from Scalp EEG Recordings

Catarina Lourenço[1,2(✉)], Marleen C. Tjepkema-Cloostermans[2,3], Luís F. Teixeira[1], and Michel J. A. M. van Putten[2]

[1] Faculty of Engineering of the University of Porto, Porto, Portugal
c.dasilvalourenco@utwente.nl, luisft@fe.up.pt
[2] University of Twente, Enschede, The Netherlands
{c.dasilvalourenco,m.j.a.m.vanputten}@utwente.nl
[3] Medisch Spectrum Twente, University of Twente, Enschede, The Netherlands
M.Tjepkema-Cloostermans@mst.nl

Abstract. Interictal Epileptiform Discharge (IED) detection in EEG signals is widely used in the diagnosis of epilepsy. Visual analysis of EEGs by experts remains the gold standard, outperforming current computer algorithms. Deep learning methods can be an automated way to perform this task. We trained a VGG network using 2-s EEG epochs from patients with focal and generalized epilepsy (39 and 40 patients, respectively, 1977 epochs total) and 53 normal controls (110770 epochs). Five-fold cross-validation was performed on the training set. Model performance was assessed on an independent set (734 IEDs from 20 patients with focal and generalized epilepsy and 23040 normal epochs from 14 controls). Network visualization techniques (filter visualization and occlusion) were applied. The VGG yielded an Area Under the ROC Curve (AUC) of 0.96 (95% Confidence Interval (CI) = 0.95 − 0.97). At 99% specificity, the sensitivity was 79% and only one sample was misclassified per two minutes of analyzed EEG. Filter visualization showed that filters from higher level layers display patches of activity indicative of IED detection. Occlusion showed that the model correctly identified IED shapes. We show that deep neural networks can reliably identify IEDs, which may lead to a fundamental shift in clinical EEG analysis.

1 Introduction

Epilepsy is the fourth most prevalent neurological disorder in the world. It is a brain disease that entails a predisposition to generate seizures, encompassing a plethora of syndromes and clinical phenomenology, some similar to other diseases [1–3]. Distinguishing a non-epileptic paroxysmal event from a seizure is clinically difficult, and the rate of misdiagnosis for epilepsy is reported to be up to 30% [4, 5]. This may result in an increased risk of recurrent seizures due to lack of adequate treatment or prescription of potentially harmful medication to patients with other disorders [6, 7].

While ictal EEGs (i.e. EEG signals recorded during seizures) can almost unequivocally distinguish an epileptic seizure from a non-epileptic one, the availability

© Springer Nature Switzerland AG 2020
J. Henriques et al. (Eds.): MEDICON 2019, IFMBE Proceedings 76, pp. 1984–1997, 2020.
https://doi.org/10.1007/978-3-030-31635-8_237

of these signals is low given that seizures occur at unknown times. In many patients, the interictal EEG (i.e. the EEG signal when no seizure is occurring) shows Interictal Epileptiform Discharges (IEDs): transient patterns that indicate an increased likelihood of seizures [1, 8, 9]. Assessment of their presence is done by visual analysis, which has been the gold standard in the clinic for almost over a century [10]. Yet, the learning curve is long, review times are significant, visual assessment is subjective and inter and intra-individual variability ranges from 5 to 25% [11, 12]. Despite these limitations, visual assessment of the EEG still outperforms current computer algorithms in detecting IEDs. These automated approaches are mostly based on 'hand-made' features that aim to mimic the characteristics used by experts in visual analysis [13–17], but they have ultimately failed to substitute the traditional approach to this task.

Deep learning methods learn from experience, creating a hierarchical representation based on raw data. Features are automatically extracted by successive layers, making artificial neural networks unbiased regarding the features used in visual analysis [17–19]. While deep neural networks are not easily interpretable, which has been pointed out as one of the drawbacks of deep learning methods [20], network probing and visualization techniques have been developed to provide some insight into the inner workings of the behavior of these models, making them more understandable and, thus, empirically reliable [21–23].

We explore whether deep neural networks can detect IEDs in EEG signals, automating EEG analysis for this task. In turn, this would render it more objective, eliminating variability and reducing the time and resources spent on this task. We also aim to provide some understanding regarding how the models reach their conclusions based on the filters and the provided inputs.

2 Methods

2.1 EEG Data and Pre-processing

EEG data from 217 patients between 4 and 72 years of age was used. The recordings were made with twenty-one silver/silver chloride cup electrodes placed on the scalp according to the international 10–20 system. All EEGs were obtained as part of routine care, and anonymized before further analysis. The patients were randomly selected from the digital database of the Medisch Spectrum Twente, in the Netherlands. This dataset included interictal EEGs from patients with focal (50 patients) and generalized (49 patients) epilepsy, containing interictal epileptiform discharges. EEGs with non-epileptiform abnormalities ("abnormal", 51 patients) and normal EEGs (67 patients) were also included. This was done based on the diagnosis from the electroencephalographers (e.g. searching for "focal epilepsy" or "normal EEG" in the conclusion of the report). The complete clinical report and the EEG recording itself were reviewed by experts (MvP and MTC). EEGs with epileptiform discharges were annotated by the experts so that IEDs could be easily identified. Epochs in which there was uncertainty regarding the occurrence of an IED were not labeled, ensuring that all the annotations corresponded to the unequivocal presence of an epileptiform discharge.

We filtered the EEG data in the 0.5–35 Hz range to reduce artefacts and down-sampled it to 125 Hz to reduce input size (and consequently computational complexity). Subsequently, the signals were re-referenced to a longitudinal bipolar montage. Each recording was split into 2 s non-overlapping epochs, yielding a 18×250 (channels $\times$ time) matrix for each epoch. The pre-processing routine was implemented in Matlab R2019a (The MathWorks, Inc., Natick, MA).

The data was randomized and split into a training/validation set containing 80% of the recordings and a test set comprised of the remaining 20%. All epochs from a patient were used either for training or testing. We applied five-fold cross validation on the training/validation set, further partitioning it in each iteration.

We created three different datasets using this method. The positive class was the same across datasets, being comprised of IEDs of focal and generalized epilepsy patients. The negative class of the first set included normal epochs from the EEGs of epilepsy patients, as well as normal EEGs (Set A). The second one was comprised only of normal EEGs (Set B), while the third included EEGs with non-epileptiform abnormalities and normal EEGs (Set C). Table 2 in the Appendix provides more details concerning the created datasets.

2.2 Deep Learning Models

A VGG C convolutional neural network (CNN) [24] was implemented in Python 2.7 using Keras 2, Theano and a CUDA-enabled NVIDIA GPU (GTX-1080), running on CentOS 7. Stochastic optimization was performed using an Adam optimizer [25] with a learning rate of $2 * 10^{-5}$, $\beta 1 = 0.91$, $\beta 2 = 0.999$, and $\varepsilon = 10^{-8}$. A sparse categorical cross entropy function was employed to estimate the loss. A batch size of 64 and weights of 100:1 were used (100 corresponding to the positive class).

2.3 Performance Evaluation

Receiver Operating Characteristic (ROC) curves were calculated for each of the cross-validation iterations using 101 discretizations. This was then averaged, yielding an average ROC curve for each set. The area under the curve (AUC) was calculated. Confidence Intervals (CIs) at 95% were calculated for the ROCs and AUCs. The sensitivity, specificity, false positive and true positive rate were assessed at a threshold where the values of sensitivity and specificity were as similar as possible (achieved by calculating the minimum of the difference) and at 99% specificity. Confidence Intervals at 95% (CIs) were calculated for these parameters. For each EEG on the test set, the sensitivity and specificity were assessed at a classification threshold of 0.5. These routines were implemented in Matlab R2019a (The MathWorks, Inc., Natick, MA).

2.4 Visualization Techniques

Filter visualization was applied by calculating and normalizing the gradients of the input with regard to the loss for each filter of each convolutional layer. Then, starting with a synthetically generated gray image with random noise with the same dimensions as the EEG epochs, gradient ascent was performed for 10 thousand iterations with a step size of 0.1.

Occlusion consisted in applying a grid to each sample and, in each iteration, setting the contents of a patch to zero, leaving the remaining sample untouched. The probability resulting from the network's prediction was stored in the center of the occluded patch so that it could be compared to the prediction without occlusion. After going through the whole image, the difference between the value in each grid patch center and the original prediction of the network was calculated. The patches with higher differences were plotted with warmer colors. The dimensions of the grid varied between 10 and 50 for the time axis and between 1 and 6 for the channel axis.

3 Results

Figure 1 shows the ROC curves yielded by the VGG model when distinguishing IEDs from normal EEG epochs (Set B). The AUC values were 0.99 (CI = 0.99 − 1.00) on the training set and 0.96 (CI = 0.95 − 0.97) on the test set. Figure 4 in the Appendix shows the analogous results for Sets A and C. When epochs containing non-epileptiform abnormalities were introduced in the dataset (Set C), the AUC value yielded by the VGG on the test set was 0.90 (CI = 0.89 − 0.90).

When IEDs were detected against the normal class (Set B), the intersection between sensitivity and specificity occurred at 98% for the training set and 93% on the test set. The true positive rates per hour were 91.03 (CI = 80.35–100.22) and 47.72 (CI = 45.60 − 49.84), respectively, with corresponding false positive rates of 22.30 (CI = 6.32 − 38.28) and 122.41 (CI = 27.63 − 217.20) (see Table 1). Increasing the specificity threshold to 99%, true positive detections became 88.71 (CI = 78.40 − 99.02) on the training set and 40.27 (CI = 38.43 − 42.12) on the test set. The false positive rates were 16.50 (CI = 4.95 − 28.06) and 32.31 (CI = 15.15 − 49.46) per hour, respectively. Table 1 also presents the equivalent values obtained when non-epileptiform abnormalities were included in the negative class (Set C).

Table 3 shows the results of the VGG using a threshold of 0.5 for the classification of each EEG on the test set of Set B (in which the network aims to distinguish IEDs from normal EEGs). Four out of the 14 patients with a normal EEG had the full EEG classified with 100% specificity (no false positive detections). The average specificity was 98.64%.

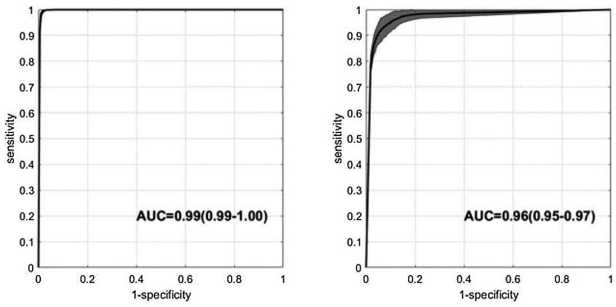

Fig. 1. ROC curves for the VGG model on the training set (left) and test set (right) of Set B. The 95% Confidence Interval (CI) of the ROC curve is shown as a shaded area. The AUC value and the corresponding CI are also presented.

Table 1. True positive and false positive rates per hour on the training and test sets of Set B and Set C. The values were assessed at a threshold where the sensitivity and specificity are equal and at a specificity of 99%. The 95% Confidence Intervals (CIs) of these rates are also presented.

Set	Spec	Sens	TP/hour	FP/hour
	Train			
B	98%[a]	98%	91.03 (80.35–100.22)	22.30 (6.32–38.28)
	99%	97%	88.71 (78.40–99.02)	16.50 (4.95–28.06)
C	85%[a]	85%	41.69 (33.75–49.62)	247.32 (116.88–377.76)
	99%	26%	12.60 (3.68-21.52)	23.14 (6.12–40.17)
	Test			
B	93%[a]	93%	47.72 (45.60–49.84)	122.41 (27.63–217.20)
	99%	79%	40.27 (38.43–42.12)	32.31 (15.15–49.46)
C	79%[a]	79%	49.30 (40.99–57.60)	348.60 (111.15–586.06)
	99%	37%	23.16 (15.10–31.22)	17.09 (1.65–32.53)

[a]sensitivity=specificity

In the focal and generalized classes (total of 20 patients on the test set), 12 patients had the full EEG classified with 100% sensitivity (all IEDs were detected). The average sensitivity and specificity values were 93.28% and 91.11%.

Considering the same analysis for Set C (which additionally included EEGs with non-epileptiform abnormalities), presented in Table 4, 4 out of the 14 patients on the test set had the full EEG classified with 100% specificity, with an average specificity of 98.47% in this class. The EEGs with non-epileptiform abnormalities (14 patients on the test set) were classified with an average specificity of 97.19%, with 100% specificity being reached for one patient. The focal and generalized IEDs (20 patients) were classified with an average sensitivity and specificity of 78.66% and 88.04%, respectively, with the IEDs of one of the patients not being detected (0% sensitivity) and the IEDs of 5 patients being detected with 100% sensitivity.

Figure 2 shows examples of the results obtained with filter visualization, which illustrate the native shape of the filters (before convolution and gradient descent). These figures can be understood as images with the same dimensions as the 2 s, 18-channel EEG epochs used as input, since those dimensions were also applied to the synthetic input used in the algorithm. Filters in lower level layers show more consistent patterns over time, while higher level layers contain filters with activity patches and low response on the remaining epoch. In the two panels of the bottom row of Fig. 2, it is possible to see that some of these patches are vertical (i.e. across channels), suggesting the detection of generalized IEDs. It is also possible to see some smaller patches, around one or two channels (e.g. upper right corner of the last filter shown in Fig. 2), suggesting the detection of focal discharges.

Figure 3 illustrates the results of occlusion with an example of each classification outcome for the set where IEDs are detected against the normal class (Set B). The scale shows the difference between the probability for each epoch and the value obtained with an occluded patch. Larger differences are plotted in warmer colors, showing that removing the patch centered in that area led to a significant change in classification, indicating that that area is important to the networks decision process. Figures 5 and 6

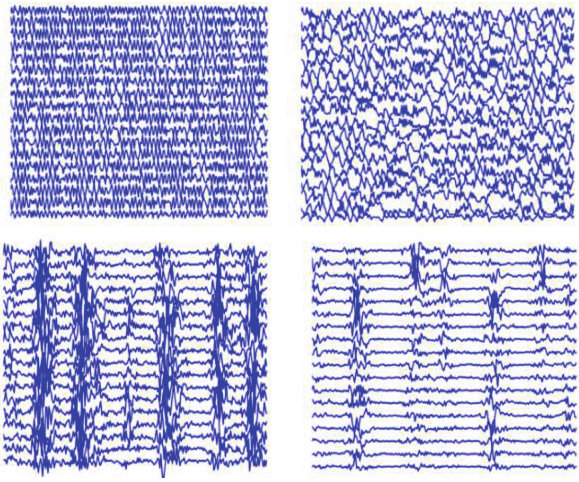

Fig. 2. Examples of results of filter visualization applied to the VGG model. The first row shows filters of lower level layers and the second row shows filters of higher level layers. These have the same dimensions as the 2 s, 18-channel EEG epochs used as input. They show the native shape of each represented filter, before any forward pass of the network.

in the Appendix show analogous examples for the set including the full EEG of epilepsy patients (Set A) and for the set containing non-epileptiform abnormalities (Set C). The detection of IED patterns in true positive cases is visible in true positive panels of Figs. 3, 5 and 6.

Comparing Fig. 6 with Figs. 3 and 5, it is possible to see that the true negative pattern corresponds to an abnormality and not to a normal EEG epoch. The false positive panel of Fig. 5 showcases an IED.

4 Discussion

We show that IEDs can be successfully identified by a VGG model. The best results were obtained when normal EEG epochs constituted the negative class (Set B). On the test set, the intersection of the values of sensitivity and specificity was at 93% and an AUC of 0.96 (CI = 0.95 − 0.97) was obtained.

Our results are up to par with the current literature regarding computer assisted IED detection, surpassing many of the described approaches. Scheuer et al. [26] applied three algorithms based on explicit feature extraction (Persyst 11, 12 and 13), obtaining sensitivities of 18%, 19% and 44%, respectively, worse than our intersection of sensitivity and specificity at 93%. Persyst 13, which yielded the highest sensitivity, detected 1.65 false positive samples per minute, which is lower than our 2.04 false positive rate per minute. However, the sensitivity threshold at which this value was calculated was vastly different. The dataset used by the authors, which consisted of records of 35 patients and 5 controls, with a total duration of 253 h, also differed greatly from ours.

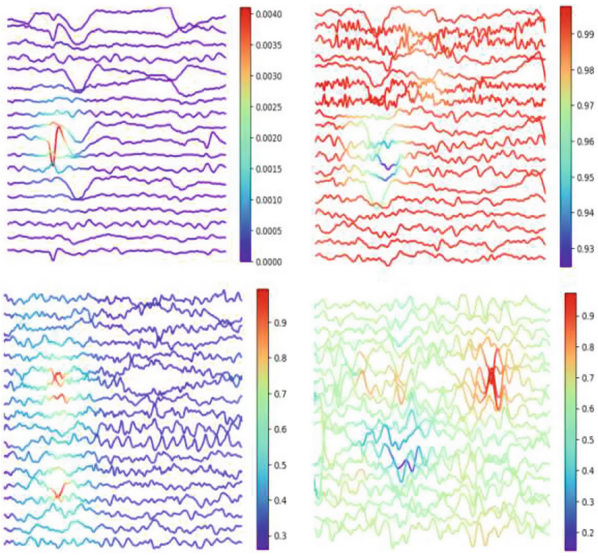

Fig. 3. Examples of the application of occlusion to the VGG model trained with set B (aiming to distinguish IEDs from Normal EEG epochs). First row: true positive (left) and true negative (right). Second row: false positive (left) and false negative (right). The scale shows the difference between the probability assigned to the epoch and what is obtained when a patch is occluded, and warmer colors are assigned to higher differences. Thus, areas plotted in warmer colors are more important for classification.

Using template matching, Lodder et al. [15] achieved 90% mean sensitivity and 2.36 false detections per minute, worse than our 2.04 false detections per minute at a sensitivity of 93%. The dataset used in Lodder et al.'s work included 20–30 min recordings from 23 epilepsy patients. With data from only 3 patients, Nonclercq et al. [16] were able to get a similar sensitivity value with template matching and k-means, again, not surpassing our results. Pang et al. [27] compared three different ANN-based methods ([13, 17, 28, 29]) using the same dataset consisting of 8 channel EEG signals from 7 epilepsy patients and 6 normal controls. This study revealed that Webber et al.'s algorithm [17], based on using mimetic features as input for a simple ANN, led to the best performance. It yielded 86.61% sensitivity and 86.32% selectivity, which is still inferior to the VGG's intersection of sensitivity and specificity at 93%.

Thomas et al. [30] used a CNN as a feature extractor, followed by an SVM as a classifier, which led to a mean AUC of 0.935 across 4 cross-validation folds, lower than the 0.96 (CI = 0.95 − 0.97) obtained on the test set by the VGG. Thomas et al.'s model was trained on 30 min recordings of 63 controls and 93 epilepsy patients. Using a 5 layer CNN as an end-to-end classifier, Johansen et al. [31] obtained an AUC of 0.947, slightly lower than the 0.96 (CI = 0.95 − 0.97) yielded by the VGG. Johansen et al. trained their network on 30 min EEG recordings from 5 epilepsy patients.

Tjepkema et al. [32] used a set of 50 patients and 50 controls to train a 19 layer, 2D CNN. The results were validated on a set of 5 patients and 12 controls, leading to 0.94 AUC for the test set, with 0.6 false detections per minute at 98% specificity.

While these results were close to those of the VGG (AUC of 0.96 and 0.5 false detections at 99% specificity), they are less reliable since the validation set is smaller.

Similarly to the approach described by Lodder et al. [33], by choosing a specificity value, the expert can limit the epochs selected for manual review. Starting with a very high threshold, only the epochs with the highest probability of containing an IED are shown. This allows the expert to diagnose a patient based on a reduced number of samples (limiting the time spent in the analysis). If these are not enough for accurate diagnosis, lowering the threshold will lead to more samples being reviewed.

We also show that the VGG can distinguish IEDs from other types of abnormalities. Abnormal EEGs were classified with an average specificity of 87.76% on the test set of set C, where abnormal EEGs (signals containing non-epileptiform abnormalities) were added to the negative class. Normal EEGs were classified with an average specificity of 98.47%, which represents a difference of less than 1% when compared to the average specificity of classification of normal EEGs on the test set of Set B. It is also important to point out that this decrease in performance was not only caused by the added complexity of the problem, but was also due to the increased class imbalance between the positive (i.e. IEDs) and negative (normal or normal and abnormal EEGs) classes, since the test set went from 8.8 h to 11.4 h and the training set increased from 24.3 h to 40.5 h, with the same number of positive samples.

The VGG model was able to detect IEDs when normal epochs from epileptic EEGs were included in the negative class (Set A), albeit with a lower performance when compared to set B (AUC of 0.91 against 0.96 on the test set of Set B, compare Figs. 1 and 4). While the increase in class imbalance contributed to this decrease in performance, similarly to what happened with the abnormal EEGs, occlusion showed that another cause for this was the mislabeling of some of the normal epochs. Figure 5 in the Appendix shows an example of a 'false positive' detection which corresponded to the occurrence of an IED. This happened since only epochs where there was no doubt about the presence of an IED were labeled. Using the information provided by this visualization technique, it was possible to account for human error and remove the normal epochs, creating Set B and improving the model's performance.

Furthermore, occlusion showed that the VGG was detecting IED shapes correctly (refer to the true positive panels of Figs. 3, 5 and 6). This result is of the utmost importance, since it proves that the network is able to classify the signal based on the correct pattern and not on spurious features, making its results more understandable and reliable.

Filter visualization provided further insight into the model's architecture, showing that filters of lower-level layers can be visually distinguished from those of higher-level layers, which include patches resembling IED detectors for focal and generalized discharges.

5 Conclusion

We show that it is possible to detect Interictal Epileptiform Discharges using a deep artificial neural network. Training a deep learning model with a larger database would contribute to an increase in model performance and robustness.

Occlusion allowed human error to be accounted for when creating the datasets and showed that IED shapes were the most important parts of the input for classification, making the classification process more transparent and contributing to the reliability of the model.

Computer assisted EEG analysis with deep learning can support clinical neurophysiologists in IED detection, reducing workload and potentially changing the way EEG interpretation is currently carried out.

Appendix

Table 2. Description of the training and test sets of each dataset, including its duration, the number of epochs and the number of epochs in the positive class (i.e. IEDs).

Set	Train			Test		
	Duration (h)	Epochs	Positive epochs	Duration (h)	Epochs	Positive epochs
A	62.6	112747	1977	13.2	23774	734
B	24.3	43867	2220	8.8	15886	452
C	40.5	72279	2015	11.4	20470	658

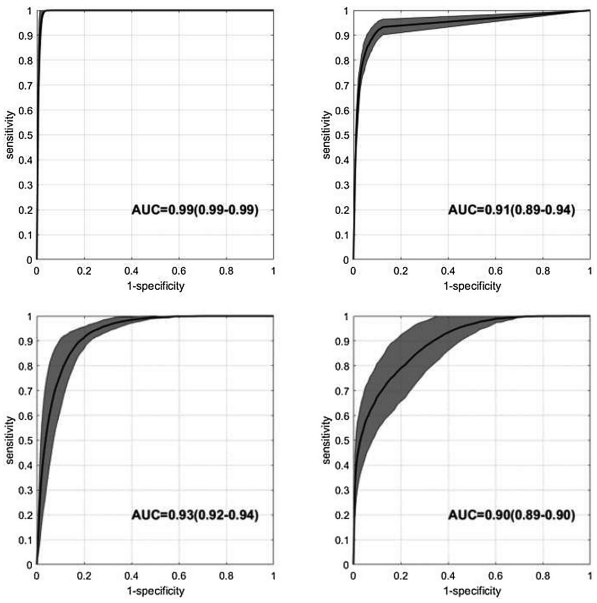

Fig. 4. ROC curves for the VGG model trained with Set A (first row) and Set C (second row). The first column shows the results on the training set and the second column shows the results on the test set. The 95% Confidence Interval (CI) of the ROC curve is shown as a shaded area. The AUC value and the corresponding CI are also presented (right).

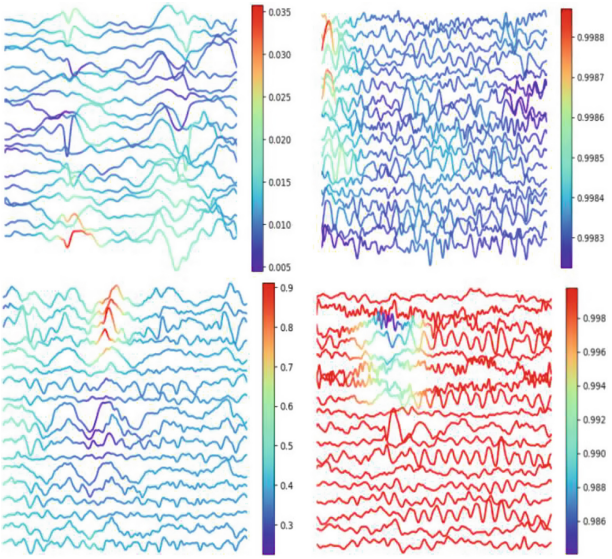

Fig. 5. Examples of the application of occlusion to the VGG model trained with set A (aiming to distinguish IEDs from Normal EEG epochs and normal epochs in epileptic EEGs). First row: true positive (left) and true negative (right). Second row: false positive (left) and false negative (right).

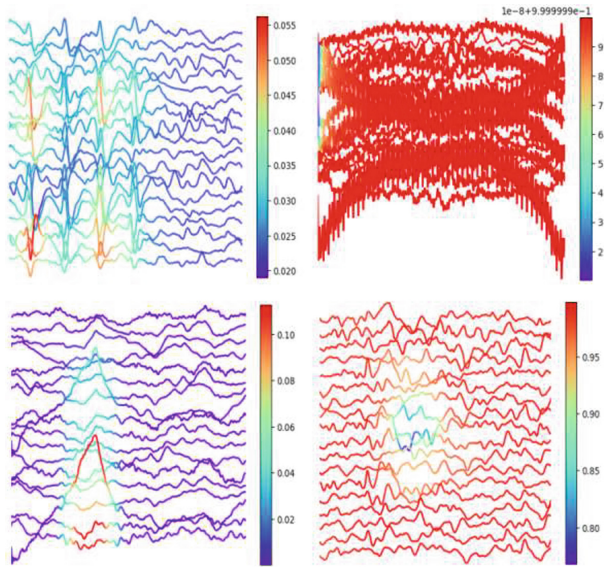

Fig. 6. Examples of the application of occlusion to the VGG model trained with set C (aiming to distinguish IEDs from Normal EEG epochs and epochs from EEGs containing non-epileptiform abnormalities). First row: true positive (left) and true negative (right). Second row: false positive (left) and false negative (right).

Table 3. Number of epochs (Epochs), number of IEDs (IEDs), Sensitivity (Sens) and Specificity (Spec) in each recording on the test set of set B, classified by the VGG with weights 100:1, at a threshold of 0.5.

	Epochs	IEDs	Sens (%)	Spec (%)
Normal	603	0	–	100.00
	538	0	–	98.88
	673	0	–	100.00
	748	0	–	95.45
	643	0	–	99.84
	598	0	–	97.49
	753	0	–	99.73
	2053	0	–	99.22
	2067	0	–	97.53
	2760	0	–	95.11
	1521	0	–	99.67
	598	0	–	97.99
	1273	0	–	100.00
	586	0	–	100.00
Focal	280	117	95.73	47.24
	1154	39	69.23	94.05
	1162	3	100.00	94.05
	204	3	66.67	95.52
	583	15	100.00	98.24
	2903	65	81.54	95.28
	665	3	100.00	99.40
	614	1	100.00	97.72
	663	10	100.00	80.86
	613	10	100.00	90.38
Generalized	618	43	97.67	87.83
	594	8	100.00	95.05
	592	9	100.00	94.34
	590	9	77.78	96.90
	626	34	91.18	95.81
	631	34	91.18	95.81
	195	4	100.00	79.06
	604	21	85.71	94.51
	588	36	100.00	88.77
	638	3	100.00	97.95

Table 4. Number of epochs (Epochs), number of IEDs (IEDs), Sensitivity (Sens) and Specificity (Spec), in each recording on the test set of set C, classified by the VGG with weights 100:1, at a threshold of 0.5.

	Epochs	IEDs	Sens (%)	Spec (%)
Normal	793	0	–	99.50
	533	0	–	98.31
	563	0	–	99.11
	673	0	–	100.00
	603	0	–	98.84
	663	0	–	99.25
	663	0	–	100.00
	593	0	–	100.00
	2053	0	–	96.64
	1895	0	–	98.63
	1723	0	–	97.34
	598	0	–	92.47
	1273	0	–	100.00
	610	0	–	98.52
Abnormal	623	0	–	91.49
	658	0	–	100.00
	533	0	–	97.75
	393	0	–	87.79
	668	0	–	97.01
	429	0	–	94.33
	477	0	–	99.16
	637	0	–	99.37
	512	0	–	96.09
	633	0	–	97.00
	981	0	–	91.03
Focal	577	39	69.23	93.49
	523	95	36.84	94.86
	611	5	80.00	98.18
	883	11	63.64	94.61
	534	67	91.04	86.08
	606	3	100.00	98.01
	639	53	0.00	99.83
	550	43	46.51	91.72
	581	23	86.96	70.61
	612	6	66.67	99.34
Generalized	618	43	100.00	85.22
	594	8	87.50	95.39
	654	20	100.00	71.29
	489	122	88.52	72.48
	195	4	100.00	61.16
	589	11	100.00	93.77
	604	21	76.19	94.34
	1121	34	94.12	89.33
	614	12	91.67	97.67
	510	89	94.38	73.40

References

1. Da Silva, F.L., Blanes, W., Kalitzin, S.N., Parra, J., Suffczynski, P., Velis, D.N.: Epilepsies as dynamical diseases of brain systems: basic models of the transition between normal and epileptic activity. Epilepsia **44**, 72–83 (2003)
2. Fisher, R.S.: ILAE official report: a practical clinical definition of epilepsy. Epilepsia **55**(4), 475–482 (2014)
3. Tatum, W.: Clinical utility of EEG in diagnosing and monitoring epilepsy in adults. Clin. Neurophysiol. **129**(5), 1056–1082 (2018)
4. Beach, R., Reading, R.: The importance of acknowledging clinical uncertainty in the diagnosis of epilepsy and non-epileptic events. Arch. Dis. Child. **90**(12), 1219–1222 (2005)
5. Zaidi, A., Clough, P., Cooper, P., Scheepers, B., Fitzpatrick, A.P.: Misdiagnosis of epilepsy: many seizure-like attacks have a cardiovascular cause. J. Am. Coll. Cardiol. **36**(1), 181–184 (2000)
6. Nowack, W.J.: Epilepsy: a costly misdiagnosis. Clin. Electroencephalogr. **28**(4), 225–228 (1997)
7. Torres, F.: Atlas and classification of electroencephalography. Pediatr. Neurol. **22**(4), 332 (2000)
8. Pillai, J., Sperling, M.R.: Interictal EEG and the diagnosis of epilepsy. Epilepsia **47**, 14–22 (2006)
9. Smith, S.: EEG in the diagnosis, classification, and management of patients with epilepsy. J. Neurol. Neurosurg. Psychiatry **76(**Suppl. 2), ii2–ii7 (2005)
10. Lodder, S.S., Askamp, J., van Putten, M.J.: Computer-assisted interpretation of the EEG background pattern: a clinical evaluation. PLoS ONE **9**(1), e85966 (2014)
11. Lodder, S.S., van Putten, M.J.: Automated EEG analysis: characterizing the posterior dominant rhythm. J. Neurosci. Methods **200**(1), 86–93 (2011)
12. Lodder, S.S., van Putten, M.J.: Quantification of the adult EEG background pattern. Clin. Neurophysiol. **124**(2), 228–237 (2013)
13. Artameeyanant, P., Chiracharit, W., Chamnongthai, K.: Spike and epileptic seizure detection using wavelet packet transform based on approximate entropy and energy with artificial neural network. In: The 5th 2012 Biomedical Engineering International Conference, pp. 1–5. IEEE (2012)
14. Liu, Y.-C., Lin, C.-C., Tsai, J.-J., Sun, Y.-N.: Model-based spike detection of epileptic EEG data. Sensors **13**(9), 12536–12547 (2013)
15. Lodder, S.S., Askamp, J., van Putten, M.J.: Inter-ictal spike detection using a database of smart templates. Clin. Neurophysiol. **124**(12), 2328–2335 (2013)
16. Nonclercq, A., et al.: Cluster-based spike detection algorithm adapts to interpatient and intrapatient variation in spike morphology. J. Neurosci. Methods **210**(2), 259–265 (2012)
17. Webber, W., Litt, B., Wilson, K., Lesser, R.P.: Practical detection of epileptiform discharges (EDs) in the EEG using an artificial neural network: a comparison of raw and parameterized EEG data. Electroencephalogr. Clin. Neurophysiol. **91**(3), 194–204 (1994)
18. LeCun, Y., Bengio, Y., Hinton, G.: Deep learning. Nature **521(**7553), 436 (2015)
19. Schmidhuber, J.: Deep learning in neural networks: an overview. Neural Netw. **61**, 85–117 (2015)
20. Qin, Z., Yu, F., Liu, C., Chen, X.: How convolutional neural network see the world-A survey of convolutional neural network visualization methods. arXiv preprint arXiv:1804.11191 (2018)

21. Nguyen, A., Yosinski, J., Clune, J.: Multifaceted feature visualization: Uncovering the different types of features learned by each neuron in deep neural networks. arXiv preprint arXiv:1602.03616 (2016)
22. Yosinski, J., Clune, J., Nguyen, A., Fuchs, T., Lipson, H.: Understanding neural networks through deep visualization. arXiv preprint arXiv:1506.06579 (2015)
23. Zeiler, M.D., Fergus, R.: Visualizing and understanding convolutional networks. In: European Conference on Computer Vision, pp. 818–833. Springer (2014)
24. Simonyan, K., Zisserman, A.: Very deep convolutional networks for large-scale image recognition. arXiv preprint arXiv:1409.1556 (2014)
25. Kingma, D.P., Ba, J.: Adam: a method for stochastic optimization. arXiv preprint arXiv:1412.6980 (2014)
26. Scheuer, M.L., Bagic, A., Wilson, S.B.: Spike detection: inter-reader agreement and a statistical turing test on a large data set. Clin. Neurophysiol. **128**(1), 243–250 (2017)
27. Pang, C.C., Upton, A.R., Shine, G., Kamath, M.V.: A comparison of algorithms for detection of spikes in the electroencephalogram. IEEE Trans. Biomed. Eng. **50**(4), 521–526 (2003)
28. Kalayci, T., Ozdamar, O.: Wavelet preprocessing for automated neural network detection of EEG spikes. IEEE Eng. Med. Biol. Mag. **14**(2), 160–166 (1995)
29. Özdamar, Ö., Kalayci, T.: Detection of spikes with artificial neural networks using raw EEG. Comput. Biomed. Res. **31**(2), 122–142 (1998)
30. Thomas, J., Comoretto, L., Jin, J., Dauwels, J., Cash, S.S., Westover, M.B.: EEG CLassification via convolutional neural network-based interictal epileptiform event detection. In: 2018 40th Annual International Conference of the IEEE Engineering in Medicine and Biology Society (EMBC), pp. 3148–3151. IEEE (2018)
31. Johansen, A.R., Jin, J., Maszczyk, T., Dauwels, J., Cash, S.S., Westover, M.B.: Epileptiform spike detection via convolutional neural networks. In: 2016 IEEE International Conference on Acoustics, Speech and Signal Processing (ICASSP), pp. 754–758. IEEE (2016)
32. Tjepkema-Cloostermans, M.C., de Carvalho, R.C., van Putten, M.J.: Deep learning for detection of focal epileptiform discharges from scalp EEG recordings. Clin. Neurophysiol. **129**(10), 2191–2196 (2018)
33. Lodder, S.S., van Putten, M.J.: A self-adapting system for the automated detection of interictal epileptiform discharges. PLoS ONE **9**(1), e85180 (2014)